Nanoscale

PAPER

View Article Online
View Journal | View Issue

Cite this: *Nanoscale*, 2023, **15**, 10295

Nanoscale chemical patterning of graphite at different length scales†

Sasikumar Rahul, [a] Miriam C. Rodríguez González, [a] Shingo Hirose,[b] Hiromasa Kaneko,[b] Kazukuni Tahara, *[b] Kunal S. Mali *[a] and Steven De Feyter *[a]

Received 10th February 2023,
Accepted 30th May 2023

DOI: 10.1039/d3nr00632h

rsc.li/nanoscale

Chemical patterning surfaces is relevant in several different domains of science and technology with exciting possibilities in electronics, catalysis, sensing, and photonics. Here, we present a novel strategy for chemical patterning of graphite using a combination of covalent and non-covalent approaches. Building on our previous work, where self-assembled monolayers of linear alkanes were used as sacrificial masks for directing the covalent anchoring of aryl groups to the graphite surface in sub-10 nm arrays, we present a modified design of a template alkane with alkoxy terminal groups which allowed better pattern transfer fidelity in comparison to simple linear alkanes. We also explored the use of chronoamperometry (CA) instead of previously used cyclic voltammetry (CV) for the functionalization process, which enabled patterning of the graphite surface at two-different length scales: few hundred nanometer circular patterns interspersed with sub-10 nm linear arrays. The covalent chemical patterning process has been studied in detail using CV and CA measurements whereas the patterned substrates have been thoroughly characterized using Raman spectroscopy, scanning tunnelling microscopy (STM) and atomic force microscopy (AFM). Based on the comparison between the pattern transfer fidelity of previously studied alkanes and newly synthesized alkoxy alkane, we discuss plausible molecular mechanism of pattern transfer.

Introduction

Nanostructured materials, with lateral dimensions typically in the range of 1–100 nm, have attracted significant attention in recent years. The surge of interest in nanostructuring of materials stems from the remarkable properties that arise due to confinement effects. Staggering developments in materials science where nanostructuring has been shown to influence catalysis,[1] energy conversion[2] and storage,[3] plasmonic behavior,[4] cell adhesion,[5] antimicrobial properties[6] are a testimony of the positive impact of nanostructured materials in science and technology.

Given the growing appreciation of nanostructured materials, strategies that allow patterning at nano to micrometer scale are highly desirable. Various methods, that employ both top-down and bottom-up approaches, such as photolithography,[7] dip-pen lithography,[8] nanografting,[9] self-assembly,[10] *etc.* have been used for the fabrication of nanostructured surfaces. While self-assembly provides relatively straightforward access to sub-5 nm periodicities,[10,11] it is arguably not the most robust patterning method due to limited stability of the self-assembled structures to environmental/experimental conditions such as solvent treatment and temperature variations. Covalent modification, where one binds organic functional groups to surfaces *via* covalent bonds, offers a robust alternative to patterning *via* self-assembly and has been traditionally used for tuning various physico-chemical properties of materials.

In this context, a particularly well-studied class is that of carbon (nano)materials. Numerous strategies for the covalent modification of carbon materials such as graphite, graphene and carbon nanotubes have been developed over the years for tuning their hydrophilicity, solubility, electronic and electrical properties, and biocompatibility.[12] While several different chemistries for covalent modification of carbon materials have been established,[13] there exist fewer examples where nanoscale spatial control over the covalent binding of functional groups was demonstrated. Such spatial control is often challenging due to the highly reactive nature of intermediates involved in the functionalization process. Reaction intermediates such as aryl radicals formed in these reactions are thermodynamically

[a]*Division of Molecular Imaging and Photonics, Department of Chemistry, KU Leuven, Celestijnenlaan 200F, 3001 Leuven, Belgium. E-mail: kunal.mali@kuleuven.be, steven.defeyter@kuleuven.be*
[b]*Department of Applied Chemistry, School of Science and Technology, Meiji University, 1-1-1 Higashimita, Tama-ku, Kawasaki, Kanagawa 214-8571, Japan. E-mail: tahara@meiji.ac.jp*

† Electronic supplementary information (ESI) available. See DOI: https://doi.org/10.1039/d3nr00632h

'short-sighted', and hence are not easily convinced towards an ordered arrangement with lower entropy.

Ordered patterns of covalently bound functional groups on graphene, graphite and other carbon surfaces have been created in the recent past. A combination of top-down and bottom-up approaches involving e-beam lithography and covalent functionalization has been employed for creating micrometer scale chemical patterns on graphene.[14,15] Another strategy involves the use of the masking effect of self-assembled polystyrene beads during the covalent functionalization process. This ensures that the covalent binding does not occur in areas blocked by the beads. Typical periodicities reached *via* this approach are up to few hundred nm.[16–18] Laser induced covalent chemical patterning of graphene has also been demonstrated recently.[19,20] These strategies have provided efficient chemical patterning with periodicities within the range of few micrometers to few hundred nanometers.[21,22]

Despite the aforementioned examples, creation of covalent chemical patterns at the lower end of the nanoscale remains a challenge. In this context, molecular self-assembly is still relevant as it routinely provides ordered structures with sub-5 nm periodicities.[23,24] Our group[25–27] and others[28–30] have developed strategies for transferring the order and the periodicities of physisorbed self-assembled molecular networks (SAMNs) to chemisorption based chemical patterning. These strategies can be divided into two categories. One, where a physisorbed network is used as a sacrificial mask for directing the binding of the reactive intermediates to the surface and the second, where the reactive moiety is a part of the self-assembling molecules. In both cases, the periodicity of the self-assembling systems is 'imprinted' in the chemical pattern.

The first strategy follows the seminal work of Buck and co-workers where a porous physisorbed SAMN was used as a template for directing the attachment of alkylthiols to the surface of Au.[28] We have developed a similar strategy for relatively unreactive substrates such as graphite and graphene where lamellar,[25] hexagonal[26] and quadratic[27] chemical patterns with periodicities lower than 10 nm were obtained *via* reductive decomposition of diazonium salts. The second strategy has also been implemented efficiently for producing patterns at the lower end of the nanoscale however requires design of special systems that can undergo self-assembly in the first step and react with the substrate in the second. Using this approach, the periodicity of the lamellar patterns formed by an alkyl substituted aniline derivative was transferred to the covalent pattern by diazotization and subsequent grafting onto the graphite surface.[29] Similarly, maleimide chemistry was used for producing hexagonal chemical patterns on graphene *via* a photocycloaddition reaction.[30] Another interesting report used the characteristic Moiré pattern of graphene on certain metals for patterned chemisorption of hydrogen onto graphene.[31–33]

Here we report on the simultaneous fabrication of geometrically dissimilar chemical patterns on the surface of graphite using the same supramolecular template. This work builds upon the foundations laid in our previous reports[25–27] and demonstrates a template-assisted covalent chemical patterning with improved pattern-transfer fidelity and control over surface architecture (Scheme 1). In contrast to our previous work where linear alkanes were used as templates,[25] in this study we employ a modified design in which the templating molecule is substituted with a terminal methoxy group. We hypothesize that the methoxy substitution would result in greater mobility of the molecular templates during the electrochemical grafting process and influence the pattern transfer. The template-assisted covalent grafting was carried out using two different electrochemical methods namely, cyclic voltammetry (CV) and chronoamperometry (CA). Covalently modified surfaces prepared using CA revealed an interesting pattern imprinting where the linear patterns (periodicities 5–6 nm) were intermixed/interrupted by circular disks of pristine areas (diameter 100–300 nm). We also discuss the effect of potential applied during CA on the nanopatterns. The functionalized substrates were characterized using Raman spectroscopy for confirming the covalent binding of the aryl units whereas the nanoscale morphology was thoroughly studied using scanning tunnelling (STM) and atomic force microscopy (AFM).

Results and discussion

Scheme 1 summarises the approach used in this work which employs a physisorbed SAMN formed by 1,40-dimethoxytetracontane (**DMTC**, Fig. 1) as a sacrificial mask for directing the binding of aryl radicals produced *via* electrochemical reduction of diazonium salts[34] to the graphite surface. Our previous work has established that the presence of a solution double layer consisting of an aqueous solution of diazonium salt (light blue, Fig. 1b) and a thin film of an organic templating phase-in which the SAMN is physisorbed on the surface (red, Fig. 1b), is necessary for efficient transfer of the pattern. The organic interface allows slight mobility within the otherwise close-packed alkyl template layer and in turn exposes the surface to aryl radicals produced during the electrolysis of the diazonium salt. We have also previously demonstrated that dry films of typical alkanes such as *n*-pentacontane ($C_{50}H_{102}$) act as excellent masks for blocking the covalent grafting of aryl radicals.[35] 3,5-Bis-*tert*-butyl benzene diazonium (TBD) chloride, an archetypal diazonium salt, was used in this study as it allows discrete grafting of single aryl units without the possibility of dendritic growth.[36] A modified template, namely **DMTC** was employed. We reasoned that the introduction of a terminal methoxy group will lead to increased mobility in the termini of the self-assembled columns thereby providing improved pattern transfer fidelity.

Prior to their use as a template for covalent chemical patterning of graphite, the self-assembled networks of **DMTC** were thoroughly characterized using STM. Fig. 1a shows the STM image of the physisorbed SAMN formed by **DMTC** at the tetradecane/HOPG interface. Similar to related alkanes, **DMTC** assembles into a columnar arrangement where molecules are

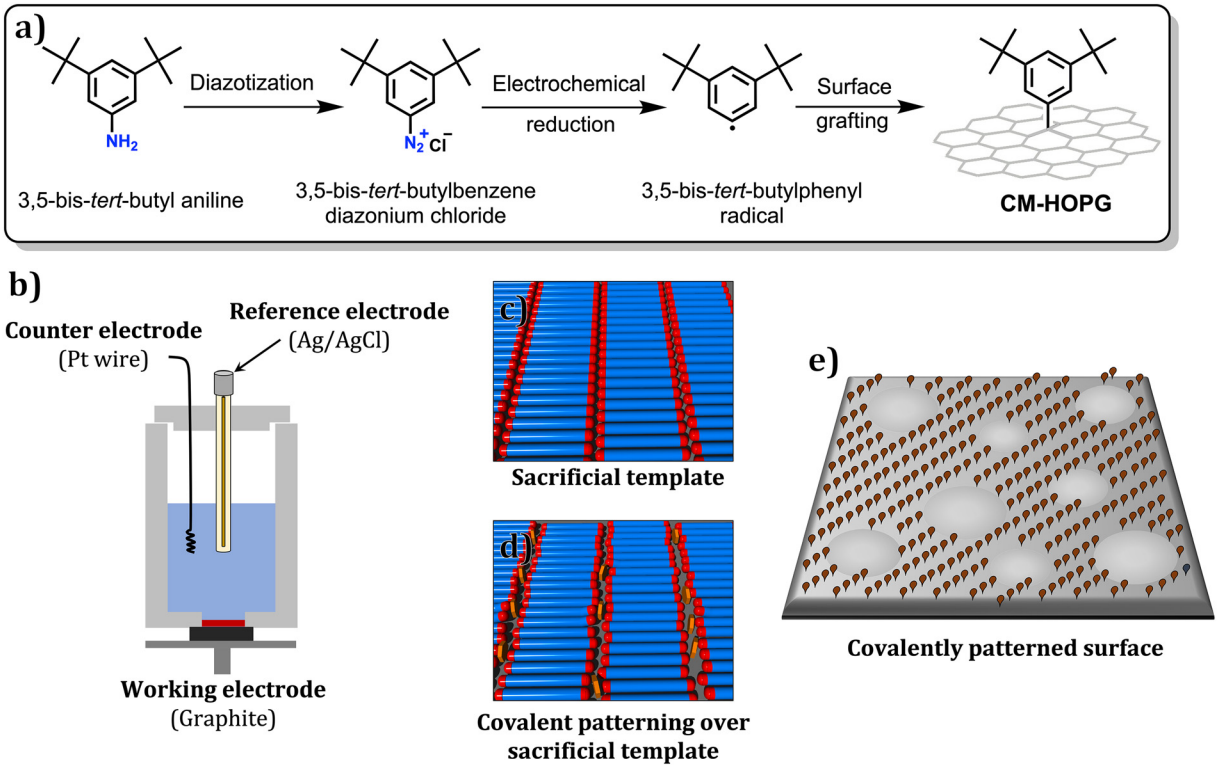

Scheme 1 (a) Reaction scheme showing the functionalization protocol used for attaching aryl groups to the surface of graphite to yield covalently modified graphite (CM-HOPG). (b) Schematic of an electrochemical cell used for covalent patterning experiments. The cell contains a solution double layer consisting of an aqueous solution of diazonium salt (light blue) and a thin film of an organic templating phase (red). The templating phase contains a monolayer of an alkoxyalkane physisorbed at the interface between a thin film of 1-phenyloctane and graphite. (c and d) Schematics showing the lamellar sacrificial template (c) and grafted aryl groups (orange disks) in between the lamellae (d). (e) Schematic showing the geometrically dissimilar nanoscale patterning achieved using the templated chemical patterning approach presented in this work.

close packed into lamellae *via* van der Waals interactions. Within each column, each molecule is adsorbed with its long axis oriented at 85 ± 2° with respect to the column axis. The width of the **DMTC** columns is 4.8 ± 0.2 nm. The darker troughs running along the column axis are the regions where the methoxy termini are adsorbed. The ether oxygens could not be identified from the STM images, possibly due to their terminal position and the anticipated mobility of the methoxy groups.[37,38] Large scale images (see Fig. S1 in the ESI†) indicate that domains spanning areas as larger as 500 × 500 nm^2 are formed under typical experimental conditions.

Following the published protocol, the ability of **DMTC** to guide aryl radical grafting on HOPG was first evaluated using CV.[25] After preparation of the solution double layer on graphite, the electrochemical reduction of TBD was induced by carrying out three iterative sweeps in CV (Fig. 1c) from +0.7 to −0.7 V (0.1 V s^{-1}) with respect to the Ag/AgCl reference electrode. A large irreversible peak observed at around −0.28 V (black, Fig. 1c) is assigned to the reduction of TBD. The two subsequent cycles (grey, Fig. 1c) carry lower and lower current and show an anodic shift. This behavior indicates the passivation of the electrode surface upon grafting and consequently lesser and lesser covalent grafting occurs in subsequent sweeps. The graphite samples were then rinsed thoroughly with deionized water and acetonitrile and Raman spectroscopy was carried out for confirming the covalent binding of the 3,5-di-*tert*-butyl phenyl (3,5-TBP) units to the basal plane of graphite. The ratio of the intensity of the D-band (~1350 cm^{-1}) and the G-band (~1580 cm^{-1}) (I_D/I_G) was used to quantify the degree of covalent grafting. In the Raman spectrum of graphitic substrates, the D-band is activated upon incorporation of defects such as sp^3 carbon atoms within the pristine sp^2 lattice which occurs upon the addition of aryl radicals to the basal plane. The G-band on the other hand remains unaffected upon covalent functionalization and hence the I_D/I_G ratio serves as a quantitative measure of defect density and in turn the number density of the covalently bound aryl groups to the basal plane.

Fig. 1d (black) shows the Raman spectrum of the graphite surface covalently modified in the presence of the **DMTC** template. The Raman spectrum of pristine graphite is also provided as a reference (grey). The covalently modified sample clearly shows a weak D-band at ~1350 cm^{-1} indicating the covalent attachment of 3,5-TBP units to the basal plane of graphite. Analysis of the Raman data provided I_D/I_G value of 0.03 ± 0.01. As anticipated, this value is lower than that obtained in the absence of any template (0.06)[25] for the same concentration of TBD. STM images of the covalently modified

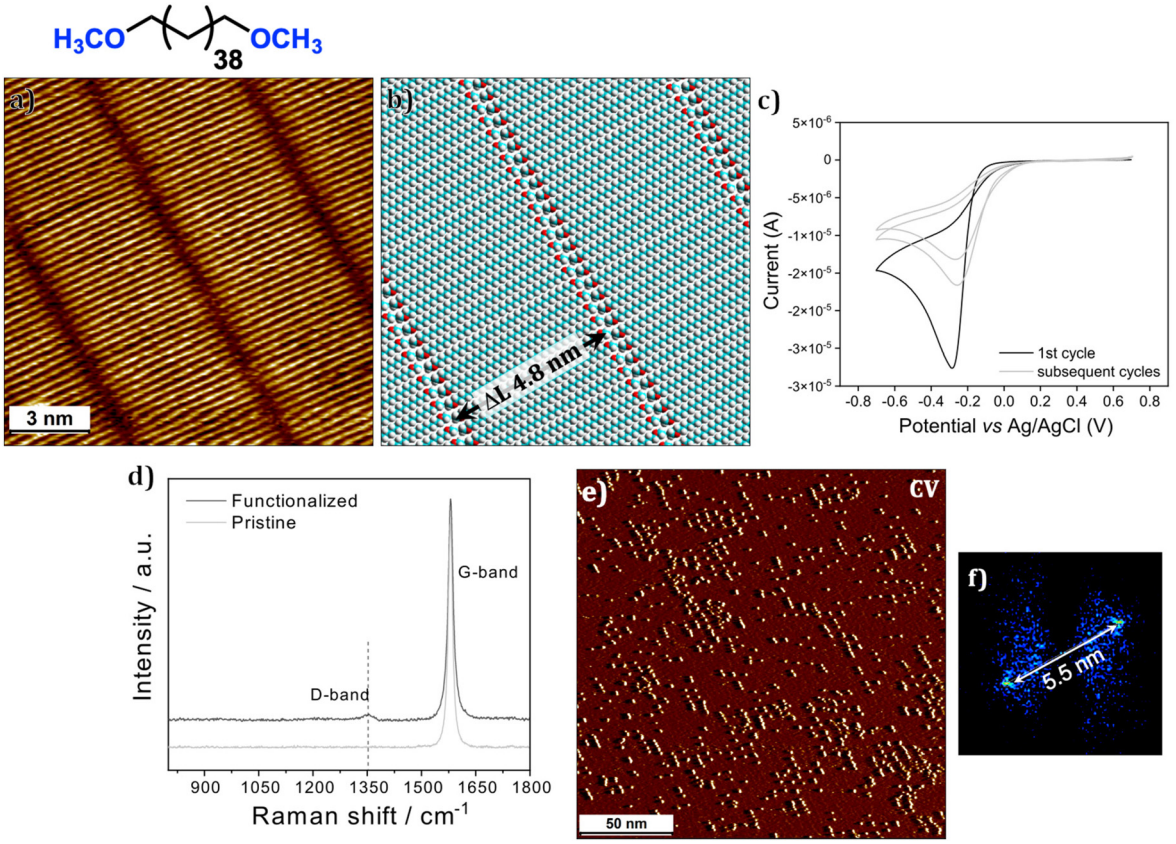

Fig. 1 (a) Small scale STM image showing the SAMN formed by **DMTC** at the tetradecane/graphite interface. Imaging conditions: V_{bias} = −0.8 V, I_{set} = 90 pA. (b) A molecular model showing the arrangement of **DMTC** molecules within the SAMN. (c) A cyclic voltammogram showing three potential sweeps revealing the reduction of the aryldiazonium salt (+0.7 to −0.7 V (scan rate = 0.1 V s^{-1}) *versus* Ag/AgCl). (d) Raman spectrum obtained after CV cycles showing emergence of a weak D-band for the covalently modified graphite sample (black). Raman spectrum of pristine graphite is also presented (grey) for the sake of comparison. (e) STM image showing linear chemical patterning achieved using **DMTC** as template. Imaging conditions: V_{bias} = −0.9 V, I_{set} = 0.04 nA. (f) 2D-fast Fourier transform (2D-FFT) spectrum of the STM image presented in panel (e).

surface clearly reveal an ordered linear arrangement of bright features (Fig. 1e) corresponding to the covalently bonded 3,5-TBP units. The periodicity of the rows was found to be 5.5 ± 0.3 nm (2D FFT, Fig. 1f) which is slightly larger than that of the DMTC template. Despite this difference, the STM data clearly confirmed that the templating ability is maintained despite the introduction of the methoxy groups to the alkane terminal.

While the periodic rows of 3,5-TBP units confirm the templating ability of the **DMTC** SAMN, the STM data does not reveal if it is better or worse than that of alkanes used in our previous work.[25,26] Below we present a systematic comparison between templating ability of pentacontane and **DMTC**. To this end, the pattern transfer fidelity of **DMTC** was quantified using a program developed in house[27] and compared to that of *n*-pentacontane. In this method, we analyze the STM images of chemically patterned surfaces for their fidelity/conformity to the pattern defined by the self-assembled template. We compare two sets of virtual distributions; the first is a representative map of $x - y$ coordinates of grafted units from STM images (*experimental coordinates*) and the second, a set of randomly generated coordinates obtained using Monte Carlo method (*random reference*). The number of points (grafted units) in both sets is kept the same. We also construct a perfect reference of the pattern for above distributions from experimentally derived parameters called a *virtual template*. The overlap of a distribution with its corresponding virtual template would scale and correlate with the pattern-transfer fidelity of grafted units on the substrate. The ratio of the number of the matched coordinates in *experimental coordinate* to that in *random reference* (E/R value) is a quantitative measure of the pattern transfer fidelity. By this definition, the E/R scores of a randomly grafted surface are distributed in a normal distribution with mean at 1. Thus, template guided patterning of the surface raises the E/R score, which increases with increasing fidelity of the pattern-transfer. Fidelity analysis of the STM data obtained on covalently functionalized samples using **DMTC**, and *n*-pentacontane revealed that the pattern transfer fidelity is better for the SAMN of **DMTC** compared to that of C_{50} (Fig. S2 in the ESI†) further validating the new design.

Having confirmed the superior templating ability of the **DMTC**, we moved on to systematically probing the influence of the number of potential cycles applied during CV on the

covalent chemical patterns. To this end, the applied potential was swept between +0.7 to −0.7 V (0.1 V s^{-1}) *versus* Ag/AgCl for one, three and five cycles (Fig. 2a–c) and the chemical patterns were characterized using STM. Fig. 2d–f shows STM images of the chemical patterns obtained using one, three and five CV cycles, respectively. The density of the grafted aryl units increases with increasing CV cycles. This was further confirmed by Raman spectroscopy which showed an increase in the I_D/I_G ratio (Fig. S3 in the ESI†). It is clearly evident from the STM data that the increase in the grafting density is manifested as non-specific, intra-pattern covalent binding wherein the aryl units are bonded in between the linear pattern created during the initial CV cycles. Specifically, comparison of Fig. 2e and f reveal that intra-pattern grafting becomes prominent after three CV cycles which essentially fills up the space in between the linear patterns. This is indicative of partial to complete desorption of **DMTC** upon repetitive potential cycling. The 2D-FFT analysis of the STM data confirmed pattern transfer by the **DMTC** template in all three cases (insets Fig. 2d–f). Note that under comparable experimental conditions, C_{50} templated surfaces do not show significant intra-pattern grafting (see Fig. S4 in the ESI†). This indicates that C_{50} template does not undergo partial desorption or at least does not exhibit similar mobility to that of **DMTC** during the electrochemical grafting process. This is in line with the original reasoning behind the design of the template in the present case.

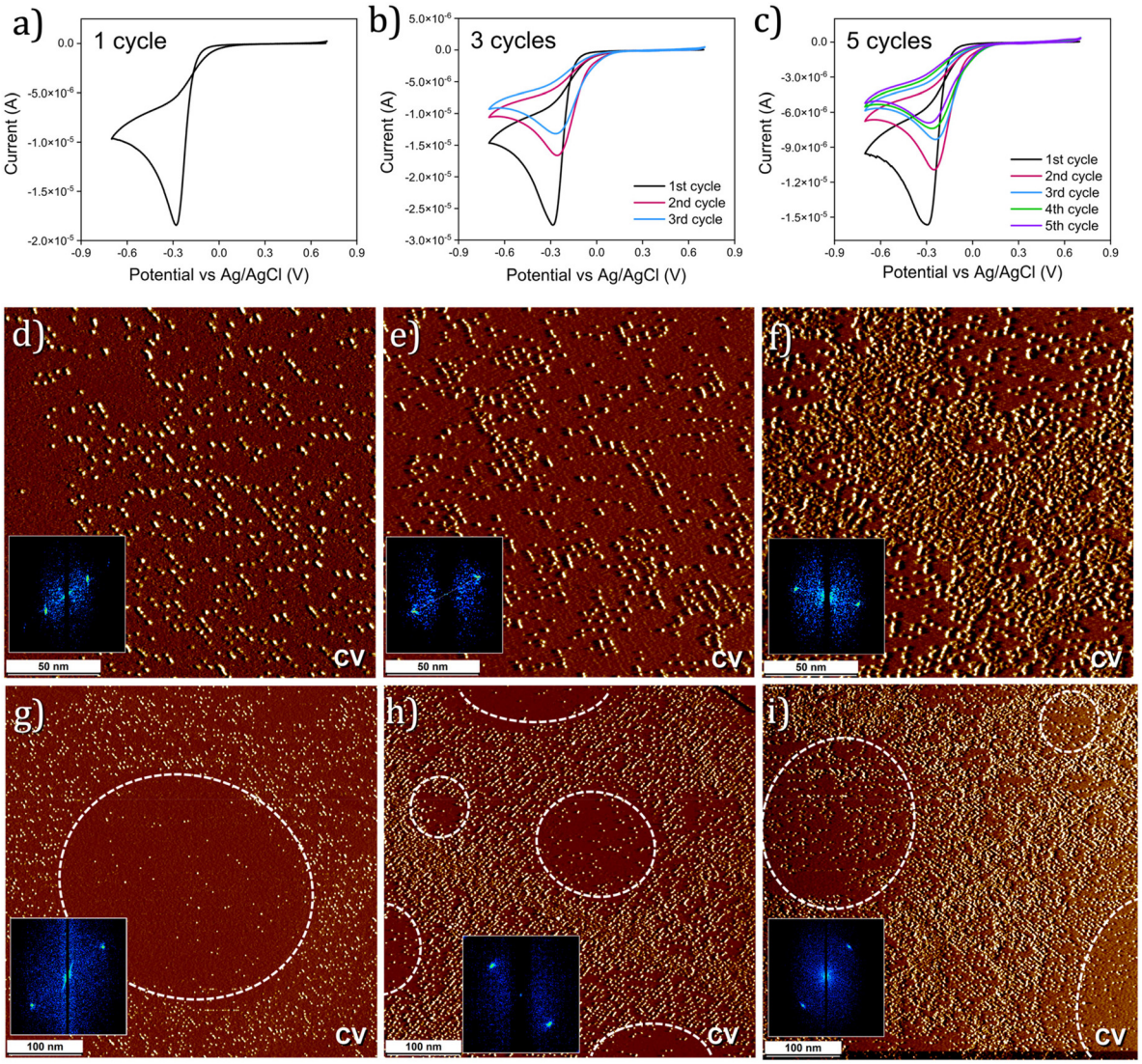

Fig. 2 Influence of the number of CV cycles on **DMTC** templated chemical patterning. (a–c) Cyclic voltammograms showing one, three and five potential sweeps between +0.7 to −0.7 V (0.1 V s^{-1}) *versus* Ag/AgCl. (d–f) STM images showing gradual increase in the grafting density with increasing CV cycles. The insets show 2D-FFT images corresponding to the STM images. (g–i) Larger scale STM images showing an additional structural feature of the chemical patterns, namely the nanocorrals, which are relatively pristine, circular areas of graphite (white dashed lines) which get filled up with grafted aryl groups with increasing CV cycles. The insets show 2D-FFT of the STM images. Imaging parameters: V_{bias} = −0.9 to −1.2 V, I_{set} = 0.04 to 0.05 nA. For additional STM data, see Fig. S5 in the ESI.†

Large scale STM images presented in Fig. 2g–i revealed another interesting feature of this system. Circular areas with low grafting density were observed within linear chemical patterns of aryl groups. The formation of such areas, the so-called corrals, was apparent already in samples prepared using one CV cycle (Fig. 2g) which get 'filled-up' with grafted units in subsequent cycles of grafting (Fig. 2f and i). We have previously reported[39] on such corrals which were observed when covalent chemical patterning was carried out using a mixture of diazonium salts. Such corrals could originate due to a combination of factors including the generation and adsorption of gaseous nanobubbles and the deposition of reaction by-products during the electrografting process. Formation of such corrals within the linear chemical patterns templated by **DMTC** is an interesting structural aspect as it represents an additional control over the chemical nanopatterning process.

In order to exert further control on the patterning process, we resorted to the use of CA. In contrast to CV, where the electrode potential is varied linearly between two limiting values as a function of time at a known sweep rate, CA applies a constant potential difference between the working and the counter electrode for a given duration. We reasoned that application of a constant, precise potential and control over time of the electrolysis through CA will provide better control over the dynamics of nanopatterning process compared to CV where the applied potential is continuously changed. To this effect, systematic CA based electrografting of **TBD** using the **DMTC** template was carried out as follows. TBD undergoes reduction at ~–0.15 V *versus* Ag/AgCl with a peak onset around −0.05 V.[36] In the presence of **DMTC** SAMN this reduction is further shifted to ~–0.25 V *versus* Ag/AgCl (Fig. 2a–c) with onset around −0.1 V. We performed CA based covalent patterning of graphite at three different overpotentials: −0.15 V, −0.35 V, and −0.60 V *versus* Ag/AgCl. Covalent grafting at these potentials was studied for short (10 s), intermediate (60 s), and long (300 s) durations of applied potential.

Fig. 3a–c shows the effect of applied potential on the chemical patterning using the **DMTC** template. The duration of applied potential was kept constant at 60 s. The STM images reveal that at −0.15 V, the surface shows linearly patterned rows of grafted TBP units and no corral formation (Fig. 3a). There is negligible intra-pattern grafting. At −0.35 V, the nanocorrals appear on the surface amongst the linearly grafted rows (Fig. 3b). The diameter of the corrals is between 100–300 nm although sizes as small as 50 nm and as large as 500 nm were also observed occasionally. The grafting density inside of the corrals is minimal and is comparable to that observed in the case of CV experiment with one cycle (Fig. 2g). Electrolysis at −0.60 V yielded a surface with comparable morphology to that observed at −0.35 V. Specifically, the surface coverage as well as the size of the corrals was found to be comparable (see Fig. S9 in the ESI†). The extent of intra-pattern grafting was found to be more pronounced at higher potentials as compared to that at −0.15 V. These results demonstrate that it is possible to control the formation of corrals *via* applied potential however the size of the corrals does not show significant dependence on the applied potential in contrast to our previous work where CA was used to control the size of the nanocorrals formed from a mixture of two diazonium salts.[39] Following the hypothesis that the corrals are templated by surface adsorbed nanobubbles of gaseous products which block grafting, a possible explanation for the disappearance of nanocorrals at the lower reducing potential could be a lower rate of bubble formation or a higher rate of bubble dissolution under these reaction conditions owing to the slower reaction kinetics at lower applied reduction potential.[40] It is also likely that the mechanism of diazonium reduction and nanobubble formation could be different in the two potential regimes separated by the peak reduction potential.

Fig. 3d–f shows the effect of the duration of applied potential (−0.60 V) on the evolution of chemical patterning. Representative large scale STM images presented in Fig. 3d–f clearly reveal the formation of corrals at all reaction times. Corrals as small as 50 nm in diameter were observed for surfaces obtained after electrolysis for 10 s. The intra-pattern grafting, which was negligible at shorter times (Fig. 3d and e), was found to become prominent at longer electrolysis times (Fig. 3f) with the rows almost entirely covered with the additional grafted molecules at 300 s. The increased extent of intra-row grafting at higher potentials and higher reaction times when seen together with the fact that large corrals remain on the surface under these conditions indicates that the nanobubble covered areas of the SAMN are relatively more stable on the surface. The Raman characterization of samples prepared under different CA conditions (Fig. 3g) revealed that the I_D/I_G ratio increases with an increase in the duration of applied potential for all three cases studied. At a given duration of electrolysis, the I_D/I_G ratio was found to increase slightly in going from −0.15 V to −0.35 V and then showed saturation or slight decrease whereas it increased steadily for the CA experiments for 300 s. These changes in grafting density are consistent with the changes in the surface morphology observed from the STM data.

To gain further insight into the morphology of the chemically patterned surfaces, AFM characterization of patterned substrates was carried out. Fig. 4a–c show AFM images of the patterned surfaces obtained in the presence of **DMTC** template at varying potentials (60 s). The larger scale morphology evident from the AFM data is consistent with that imaged using STM. The AFM image of the surface prepared at −0.15 V shows no clear evidence of corral formation. Some areas with lower surface coverage of the organic film are visible (white dashed circles, Fig. 4a) which may indicate partial blocking of grafting due to the gaseous nanobubbles in the initial stages of the reaction which are eventually removed and covered with grafted aryl groups. This observation is consistent with our hypothesis drawn from the STM data which also showed no obvious corral formation. AFM images of the samples prepared at −0.35 V, and −0.60 V (Fig. 4b and c), on the other hand, clearly revealed formation of circular corrals, the size distribution of which (80–250 nm) was found to be consistent with the STM data.

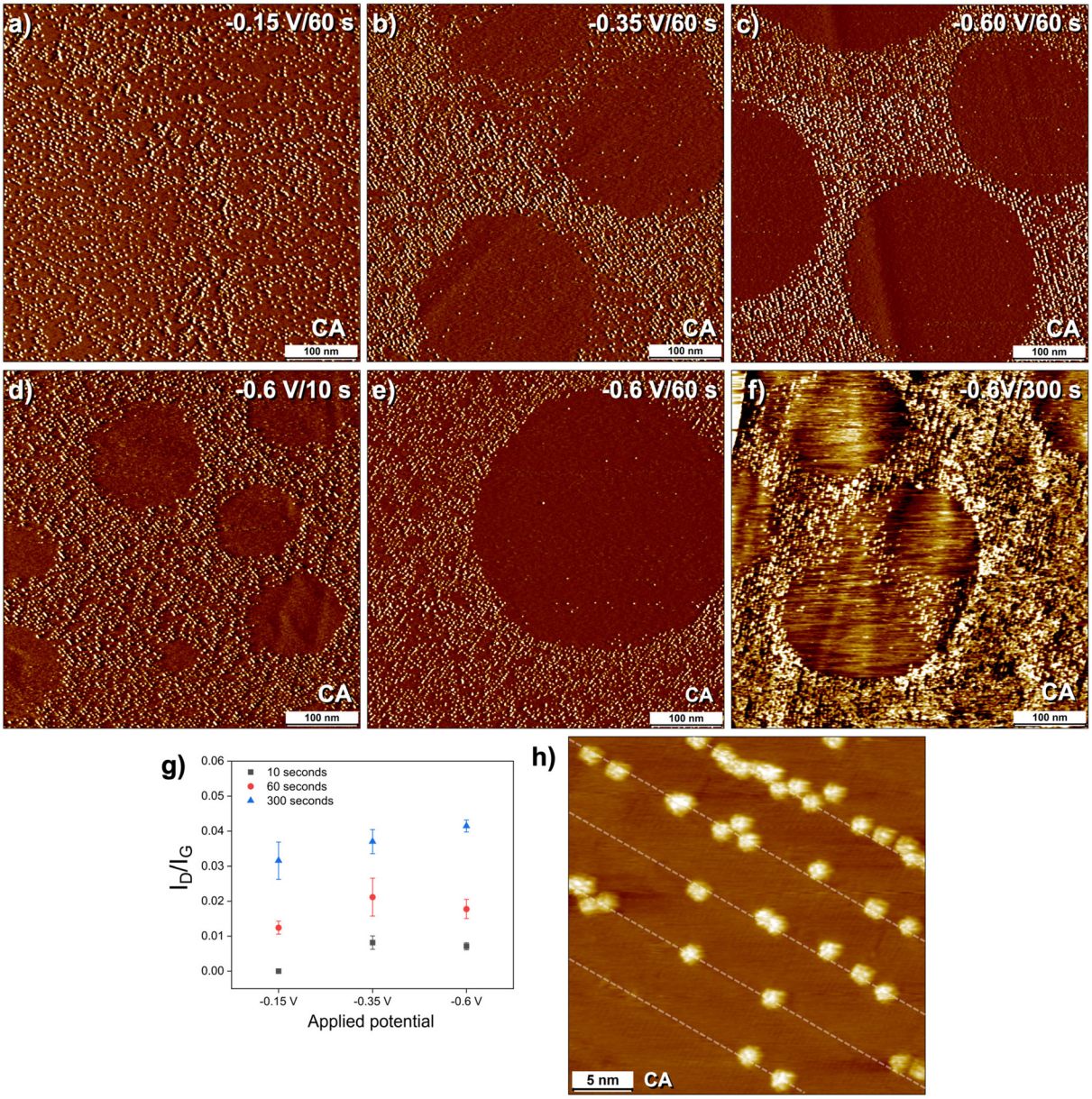

Fig. 3 (a–c) STM images showing the influence of the applied potential on the chemical patterning using **DMTC** template. The duration of the electrolysis was kept constant at 60 s for these experiments. (d–f) STM data showing the effect of electrolysis duration at a constant potential (−0.60 V). (g) A plot of I_D/I_G *versus* applied potential at different electrolysis times. (h) High-resolution STM image showing sub-molecular resolution of the covalently grafted aryl units. Careful inspection of the image also shows the presence of DMTC template monolayer in the background of grafted units. The white dashed lines serve as guide to the eye. This sample was prepared using CA (−0.35 V, 40 s). Imaging parameters: V_{bias} = −0.9 to −1.2 V, I_{set} = 0.04 to 0.05 nA. For additional STM data, see Fig. S6–S8 in the ESI.†

We also carried out CA in short pulses to understand its influence on nanocorral formation and overall morphology of the grafted surfaces. Short (2 seconds wide) pulses of −0.35 V (with an interval of 0.5 seconds at 0.62 V between the pulses) were applied to **DMTC** covered graphite surface (Fig. 5a and b). Fig. 5c and d show STM images of the patterned graphite surfaces obtained after 5 and 10 potential pulses, respectively. The STM data reveals that corrals are formed despite the short duration of the potential pulses indicating the plausible adsorption of gaseous by-products and that the potential cycling does not necessarily remove them from the surface. While there is negligible grafting inside of the corrals, we observe significant intra-pattern grafting within the rows. Coupled with observations made from previous CA experiments, these results point towards the molecular mechanism of patterned covalent grafting. At initial stages, the covalent binding occurs in a patterned fashion defined by the molecular template. Once the density of grafted units along the

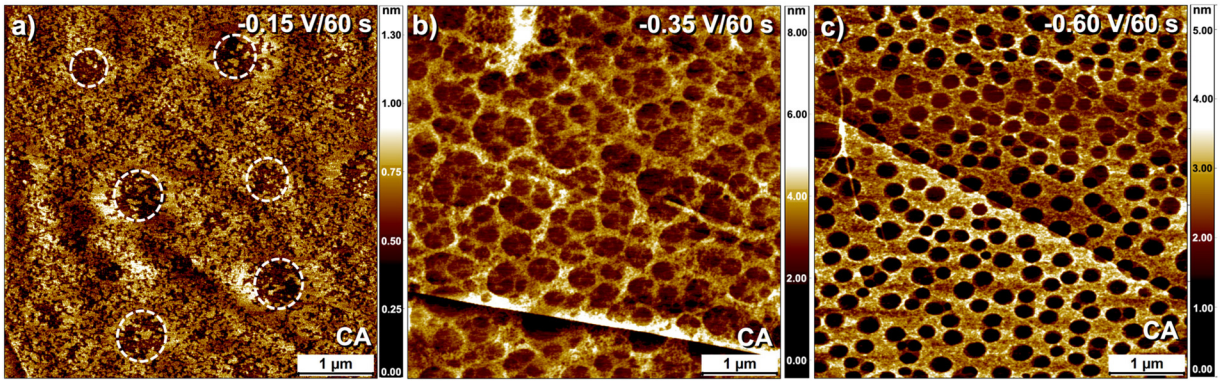

Fig. 4 Tapping mode AFM topography images of covalently patterned graphite prepared using the **DMTC** template. The samples were prepared at (a) −0.15 V; (b) −0.35 V and (c) −0.60 V. The electrolysis time was kept at 60 s for all samples. The white dashed circles in (a) highlight the areas with lower surface coverage of the organic film. For phase images see Fig. S10 in the ESI.†

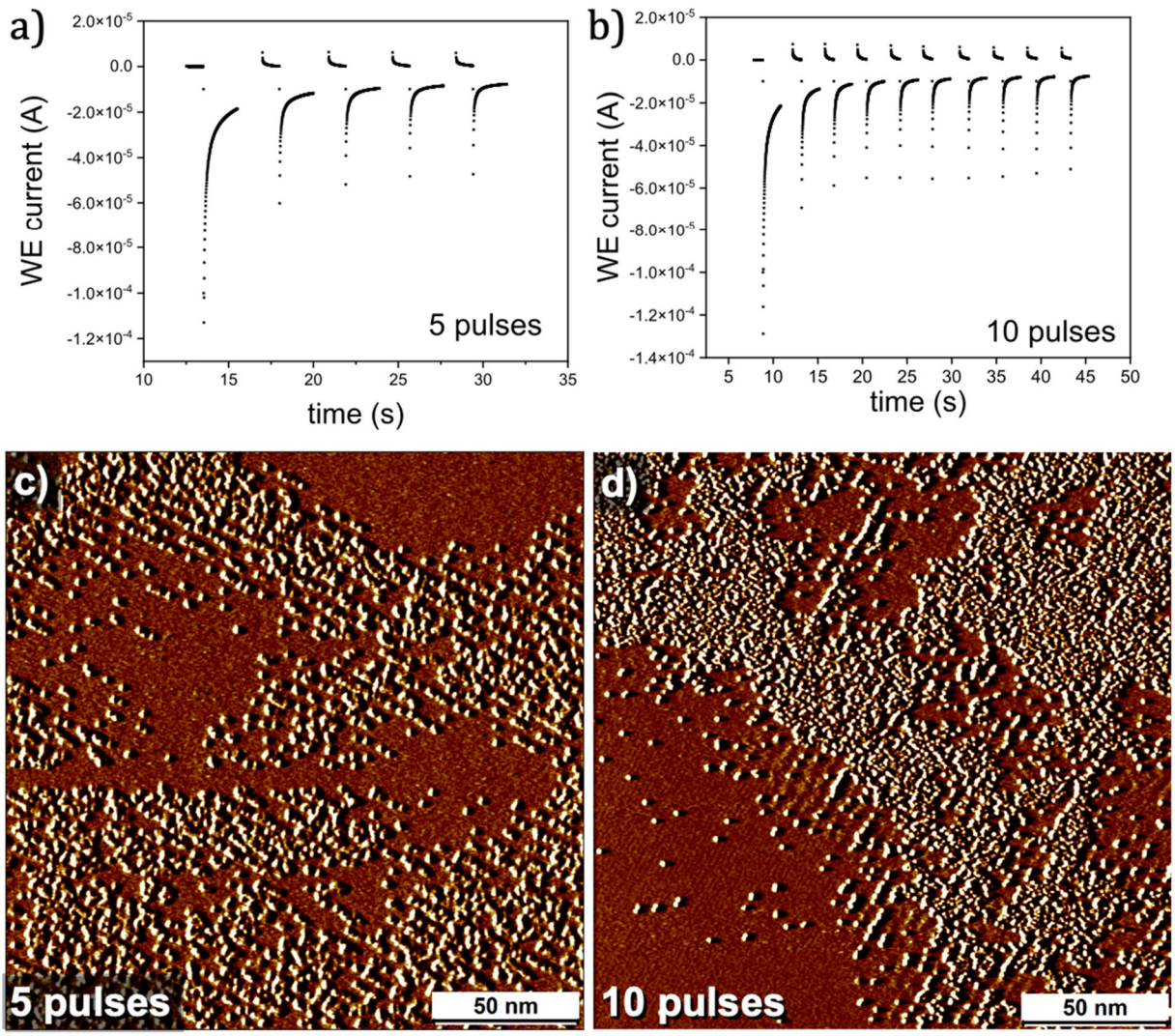

Fig. 5 CA carried out using short potential pulses. Pulse potential: −0.35 V, pulse width: 2 seconds, pulse interval: 0.5 seconds. Current profiles for (a) 5 pulses. (b) 10 pulses. (c and d) Representative STM images showing **DMTC** templated chemical patterning obtained using 5 and 10 potential pulses, respectively. Imaging parameters: V_{bias} = −0.9 V, I_{set} = 0.05 nA.

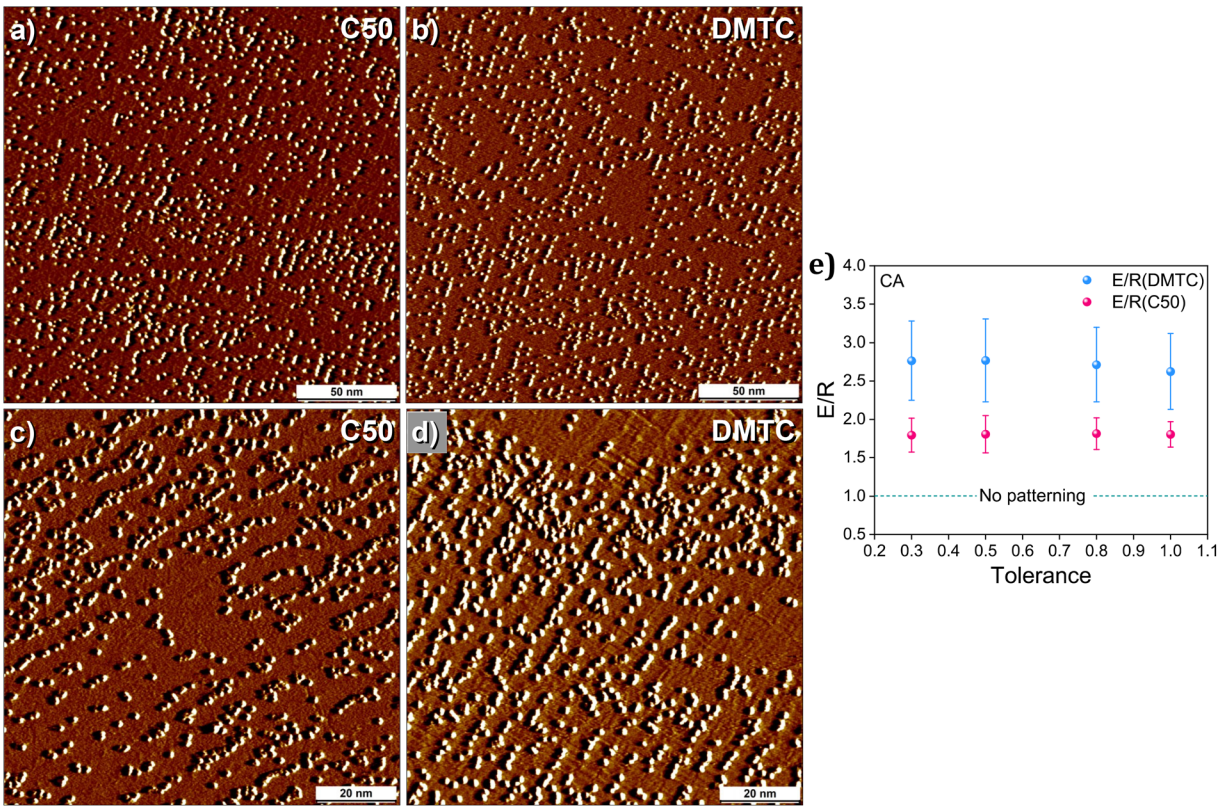

Fig. 6 Comparison of pattern transfer fidelity between **DMTC** and C_{50} templates using CA-based covalent grafting. Large (a and b) and small (c and d) scale STM images showing subtle differences in the pattern transfer fidelity of **DMTC** and C_{50}. Imaging parameters: V_{bias} = −0.9 V, I_{set} = 0.05 nA. For the same images with guiding lines, see Fig. S11 in the ESI.† (e) Calculated mean *E*/*R* values for the pattern transfer fidelity for DMTC and C_{50}. This analysis is based on 15 and 13 (200 nm × 200 nm) images for **DMTC** and C_{50}, respectively.

linear rows is saturated, there is clear preference for further covalent binding within the rows which may occur simultaneously with partial desorption of the molecular template. One could also invoke the possibility that the reactivity of the regions in-between the linearly patterned rows is slightly higher due to the sp^3 defects created in the vicinity. The systematic experimental results presented above clearly indicate the possibility of tuning the chemical patterns by precisely varying experimental conditions which in turn brought molecular insight into the process of template assisted chemical patterning.

Finally, to compare the pattern transfer fidelity of **DMTC** to that of C_{50}, CA-based covalent grafting was carried out using C_{50} as the template. Fig. 6a–d shows representative STM images for graphite substrates chemically patterned using **DMTC** and C_{50} as templates, respectively. The STM images show subtle differences in the chemical patterns indicating better pattern transfer fidelity for the former. The STM data was further subjected to detailed quantification of the pattern transfer fidelity using the program described earlier. The *E*/*R* values calculated from the fidelity analysis are plotted in Fig. 6e. The plot reveals that the *E*/*R* values are consistently higher for **DMTC** than those for C_{50} which confirms that the pattern transfer fidelity is better when **DMTC** is used as a template.

Conclusions

The chemistry of carbon surfaces has redeemed itself in recent years due to its applicability towards covalent modification of graphene and related 2D materials. In the same context, nanostructuring of such materials is under spotlight in view beneficial attributes of nanostructured materials. In the results described above, we have provided a step forward towards refining the pattern transfer fidelity of sub-10 nm chemical patterns produced *via* SAMN templating. We illustrate that the newer design of alkoxy alkane is an improved template in terms of pattern transfer fidelity in line with the anticipated increased mobility of the termini during the electrochemical grafting process. The chemical patterning was studied using both CV and CA which demonstrated better control over the process using the latter. A somewhat serendipitous observation is the simultaneous formation of circular nanocorrals interspersed within the lamellar sub-10 nm chemical patterns. We have discussed possible origins of such

pattern formation. Furthermore, comparison between the templating abilities of alkoxyalkane and previously used normal alkanes allowed us to gain insight into the mechanism of templated grafting at the molecular scale. We found out, *via* such systematic comparison, that the improved pattern transfer fidelity comes at the expense of the stability of the monolayer wherein the intra-pattern grafting was found to be relatively more prominent for the alkoxy alkane compared to the normal alkane. The improved design and the molecular insight gained will allow efficient and precise chemical patterning of (carbon) surfaces.

The improvement in the precision of chemical patterning demonstrated above bodes well not only for potential applicability of such patterned materials but also for the interesting chemistry and physics which may be associated with such nanoscale patterns as the length scale (sub-10, sub-5 nm) is within the realm of fundamental material properties such as typical molecular lengths, carrier diffusion lengths *etc*. Such long-range ordered chemical defects can potentially affect the nature of the surface, interfacial interactions, and electronic band structure of materials thereby paving way for the discovery of exotic/desirable materials properties. Furthermore, we intend to use such complex nanostructured surfaces for studying the fundamentals of molecular self-assembly. Such patterned surfaces are interesting testbeds for investigating molecular self-assembly as the two length scales are typical: one corresponding to the periodicities of SAMNs and the other to the typical domain sizes. One such study is in progress and may potentially reveal interesting information on the nucleation and growth of SAMN on nanopatterned surfaces.

Author contributions

K. T., K. S. M. and S. D. F. conceived the idea. S. H. synthesized and characterized DMTC. S. R. and M. C. R. G. planned and designed the grafting experiments. S. R. carried out the grafting experiments, characterized the grafted surfaces and performed the fidelity analysis. H. K. developed the code used for fidelity analysis. S. R. and K. S. M. wrote the manuscript with the input from all co-authors.

Conflicts of interest

There are no conflicts to declare.

Acknowledgements

Financial support from the Research Foundation-Flanders (FWO G081518N, G0A3220N) and KU Leuven–Internal Funds (C14/19/079) is acknowledged. This work was in part supported by FWO and F. R. S.-FNRS under the Excellence of Science EOS program (project 30489208 and 40007495). KT and HK thank support by JSPS KAKENHI (grant number JP20H02553).

References

1 F. Zaera, Nanostructured materials for applications in heterogeneous catalysis, *Chem. Soc. Rev.*, 2013, **42**, 2746–2762.
2 Y.-G. Guo, J.-S. Hu and L.-J. Wan, Nanostructured Materials for Electrochemical Energy Conversion and Storage Devices, *Adv. Mater.*, 2008, **20**, 2878–2887.
3 F. J. Martin-Martinez, K. Jin, D. López Barreiro and M. J. Buehler, The Rise of Hierarchical Nanostructured Materials from Renewable Sources: Learning from Nature, *ACS Nano*, 2018, **12**, 7425–7433.
4 A. Minopoli, A. Acunzo, B. Della Ventura and R. Velotta, Nanostructured Surfaces as Plasmonic Biosensors: A Review, *Adv. Mater. Interfaces*, 2022, **9**, 2101133.
5 K. Zhang, H. Gao, R. Deng and J. Li, Emerging Applications of Nanotechnology for Controlling Cell-Surface Receptor Clustering, *Angew. Chem., Int. Ed.*, 2019, **58**, 4790–4799.
6 D. P. Linklater, V. A. Baulin, S. Juodkazis, R. J. Crawford, P. Stoodley and E. P. Ivanova, Mechano-bactericidal actions of nanostructured surfaces, *Nat. Rev. Microbiol.*, 2021, **19**, 8–22.
7 J. del Barrio and C. Sánchez-Somolinos, Light to Shape the Future: From Photolithography to 4D Printing, *Adv. Opt. Mater.*, 2019, **7**, 1900598.
8 G. Liu, S. H. Petrosko, Z. Zheng and C. A. Mirkin, Evolution of Dip-Pen Nanolithography (DPN): From Molecular Patterning to Materials Discovery, *Chem. Rev.*, 2020, **120**, 6009–6047.
9 A. R. Sulkanen, M. Wang, L. A. Swartz, J. Sung, G. Sun, J. S. Moore, N. R. Sottos and G.-y. Liu, Production of Organizational Chiral Structures by Design, *J. Am. Chem. Soc.*, 2022, **144**, 824–831.
10 A. Singh, A. Shi and S. A. Claridge, Nanometer-scale patterning of hard and soft interfaces: from photolithography to molecular-scale design, *Chem. Commun.*, 2022, **58**, 13059–13070, DOI: **10.1039/D2CC05221K**.
11 K. Nickmans, R. C. P. Verpaalen, J. N. Murphy and A. P. H. J. Schenning, Sub-5 nm structured films by hydrogen bonded siloxane liquid crystals and block copolymers, *J. Mater. Chem. C*, 2018, **6**, 3042–3046.
12 T. Wei, F. Hauke and H. Andreas, Covalent Inter-Synthetic-Carbon-Allotrope Hybrids, *Acc. Chem. Res.*, 2019, **52**, 2037–2045.
13 C. K. Chua and M. Pumera, Covalent chemistry on graphene, *Chem. Soc. Rev.*, 2013, **42**, 3222–3233.
14 T. Wei, M. Kohring, M. Chen, S. Yang, H. B. Weber, F. Hauke and A. Hirsch, Highly Efficient and Reversible Covalent Patterning of Graphene: 2D-Management of Chemical Information, *Angew. Chem., Int. Ed.*, 2020, **59**, 5602–5606.
15 M. C. Rodríguez González, A. Leonhardt, H. Stadler, S. Eyley, W. Thielemans, S. De Gendt, K. S. Mali and S. De Feyter, Multicomponent Covalent Chemical Patterning of Graphene, *ACS Nano*, 2021, **15**, 10618–10627.
16 H. Van Gorp, P. Walke, A. M. Bragança, J. Greenwood, O. Ivasenko, B. E. Hirsch and S. De Feyter, Self-Assembled

Polystyrene Beads for Templated Covalent Functionalization of Graphitic Substrates Using Diazonium Chemistry, *ACS Appl. Mater. Interfaces*, 2018, **10**, 12005–12012.

17 B. P. Corgier and D. Bélanger, Electrochemical Surface Nanopatterning Using Microspheres and Aryldiazonium, *Langmuir*, 2010, **26**, 5991–5997.

18 V.-Q. Nguyen, D. Schaming, P. Martin and J.-C. Lacroix, Nanostructured Mixed Layers of Organic Materials Obtained by Nanosphere Lithography and Electrochemical Reduction of Aryldiazonium Salts, *Langmuir*, 2019, **35**, 15071–15077.

19 K. F. Edelthalhammer, D. Dasler, L. Jurkiewicz, T. Nagel, S. Al-Fogra, F. Hauke and A. Hirsch, Covalent 2D-Engineering of Graphene by Spatially Resolved Laser Writing/Reading/Erasing, *Angew. Chem., Int. Ed.*, 2020, **59**, 23329–23334.

20 S. Toyouchi, M. Wolf, G. Feng, Y. Fujita, B. Fortuni, T. Inose, K. Hirai, S. De Feyter and H. Uji-i, All-Optical and One-Color Rewritable Chemical Patterning on Pristine Graphene under Water, *J. Phys. Chem. Lett.*, 2022, **13**, 3796–3803.

21 T. Wei, L. Bao, F. Hauke and A. Hirsch, Recent Advances in Graphene Patterning, *ChemPlusChem*, 2020, **85**, 1655–1668.

22 T. Wei, F. Hauke and A. Hirsch, Evolution of Graphene Patterning: From Dimension Regulation to Molecular Engineering, *Adv. Mater.*, 2021, **33**, 2104060.

23 K. S. Mali, N. Pearce, S. De Feyter and N. R. Champness, Frontiers of supramolecular chemistry at solid surfaces, *Chem. Soc. Rev.*, 2017, **46**, 2520–2542.

24 D. P. Goronzy, M. Ebrahimi, F. Rosei, Arramel, Y. Fang, S. De Feyter, S. L. Tait, C. Wang, P. H. Beton, A. T. S. Wee, P. S. Weiss and D. F. Perepichka, Supramolecular Assemblies on Surfaces: Nanopatterning, Functionality, and Reactivity, *ACS Nano*, 2018, **12**, 7445–7481.

25 K. Tahara, T. Ishikawa, B. E. Hirsch, Y. Kubo, A. Brown, S. Eyley, L. Daukiya, W. Thielemans, Z. Li, P. Walke, S. Hirose, S. Hashimoto, S. De Feyter and Y. Tobe, Self-Assembled Monolayers as Templates for Linearly Nanopatterned Covalent Chemical Functionalization of Graphite and Graphene Surfaces, *ACS Nano*, 2018, **12**, 11520–11528.

26 K. Tahara, Y. Kubo, S. Hashimoto, T. Ishikawa, H. Kaneko, A. Brown, B. E. Hirsch, S. D. Feyter and Y. Tobe, Porous Self-Assembled Molecular Networks as Templates for Chiral-Position-Controlled Chemical Functionalization of Graphitic Surfaces, *J. Am. Chem. Soc.*, 2020, **142**, 7699–7708.

27 S. Hashimoto, H. Kaneko, S. De Feyter, Y. Tobe and K. Tahara, Symmetry and spacing controls in periodic covalent functionalization of graphite surfaces templated by self-assembled molecular networks, *Nanoscale*, 2022, **14**, 12595–12609.

28 R. Madueno, M. T. Räisänen, C. Silien and M. Buck, Functionalizing hydrogen-bonded surface networks with self-assembled monolayers, *Nature*, 2008, **454**, 618–621.

29 Z. Xia, F. Leonardi, M. Gobbi, Y. Liu, V. Bellani, A. Liscio, A. Kovtun, R. Li, X. Feng, E. Orgiu, P. Samorì, E. Treossi and V. Palermo, Electrochemical Functionalization of Graphene at the Nanoscale with Self-Assembling Diazonium Salts, *ACS Nano*, 2016, **10**, 7125–7134.

30 M. Yu, C. Chen, Q. Liu, C. Mattioli, H. Sang, G. Shi, W. Huang, K. Shen, Z. Li, P. Ding, P. Guan, S. Wang, Y. Sun, J. Hu, A. Gourdon, L. Kantorovich, F. Besenbacher, M. Chen, F. Song and F. Rosei, Long-range ordered and atomic-scale control of graphene hybridization by photocycloaddition, *Nat. Chem.*, 2020, **12**, 1035–1041.

31 J. J. Navarro, F. Calleja, R. Miranda, E. M. Pérez and A. L. Vázquez de Parga, High yielding and extremely site-selective covalent functionalization of graphene, *Chem. Commun.*, 2017, **53**, 10418–10421.

32 R. Balog, B. Jorgensen, L. Nilsson, M. Andersen, E. Rienks, M. Bianchi, M. Fanetti, E. Laegsgaard, A. Baraldi, S. Lizzit, Z. Sljivancanin, F. Besenbacher, B. Hammer, T. G. Pedersen, P. Hofmann and L. Hornekaer, Bandgap opening in graphene induced by patterned hydrogen adsorption, *Nat. Mater.*, 2010, **9**, 315–319.

33 J. J. Navarro, S. Leret, F. Calleja, D. Stradi, A. Black, R. Bernardo-Gavito, M. Garnica, D. Granados, A. L. Vázquez de Parga, E. M. Pérez and R. Miranda, Organic Covalent Patterning of Nanostructured Graphene with Selectivity at the Atomic Level, *Nano Lett.*, 2016, **16**, 355–361.

34 D. Bélanger and J. Pinson, Electrografting: a powerful method for surface modification, *Chem. Soc. Rev.*, 2011, **40**, 3995–4048.

35 Z. Li, H. Van Gorp, P. Walke, T. H. Phan, Y. Fujita, J. Greenwood, O. Ivasenko, K. Tahara, Y. Tobe, H. Uji-i, S. Mertens and S. De Feyter, Area-Selective Passivation of sp2 Carbon Surfaces by Supramolecular Self-Assembly, *Nanoscale*, 2017, **9**, 5188–5193.

36 J. Greenwood, T. H. Phan, Y. Fujita, Z. Li, O. Ivasenko, W. Vanderlinden, H. Van Gorp, W. Frederickx, G. Lu, K. Tahara, Y. Tobe, H. Uji-i, S. F. L. Mertens and S. De Feyter, Covalent Modification of Graphene and Graphite Using Diazonium Chemistry: Tunable Grafting and Nanomanipulation, *ACS Nano*, 2015, **9**, 5520–5535.

37 Y. Wei, W. Tong and M. B. Zimmt, Self-Assembly of Patterned Monolayers with Nanometer Features: Molecular Selection Based on Dipole Interactions and Chain Length, *J. Am. Chem. Soc.*, 2008, **130**, 3399–3405.

38 D. F. Padowitz, D. M. Sada, E. L. Kemer, M. L. Dougan and W. A. Xue, Molecular Tracer Dynamics in Crystalline Organic Films at the Solid–Liquid Interface, *J. Phys. Chem. B*, 2002, **106**, 593–598.

39 T. H. Phan, H. Van Gorp, Z. Li, T. M. Trung Huynh, Y. Fujita, L. Verstraete, S. Eyley, W. Thielemans, H. Uji-i, B. E. Hirsch, S. F. L. Mertens, J. Greenwood, O. Ivasenko and S. De Feyter, Graphite and Graphene Fairy Circles: A Bottom-Up Approach for the Formation of Nanocorrals, *ACS Nano*, 2019, **13**, 5559–5571.

40 Y. Ma, Z. Guo, Q. Chen and X. Zhang, Dynamic Equilibrium Model for Surface Nanobubbles in Electrochemistry, *Langmuir*, 2021, **37**, 2771–2779.